Stable polyglutamine dimers can contain β-hairpins with interdigitated sidechains—but not α-helices, β-nanotubes, β-pseudohelices, or steric zippers

Markus S. Miettinen[a,b], Luca Monticelli[c,d,e], Praveen Nedumpully Govindan[f], Volker Knecht[g] and Zoya Ignatova[b]

[a] Fachbereich Physik, Freie Universität Berlin, 14195 Berlin, Germany
[b] Institute of Biochemistry and Biology, University of Potsdam, Karl-Liebknecht-Str. 24-25, 14476 Potsdam, Germany
[c] INSERM, UMR-S665, Paris, F-75015, France*
[d] Université Paris Diderot, Sorbonne Paris Cité, UMR-S665, Paris, F-75013, France*
[e] INTS, Paris, F-75015, France*
[f] Department of Applied Physics, Aalto University, P. O. Box 11100, FI-00076 Aalto, Finland†
[g] Department of Theory and Bio-Systems, Max Planck Institute of Colloids and Interfaces, Am Mühlenberg 1, 14476 Potsdam, Germany‡

Abstract

A common thread connecting nine fatal neurodegenerative protein aggregation diseases is an abnormally expanded polyglutamine tract found in the respective proteins. Although the structure of this tract in the large mature aggregates is becoming increasingly well described, its structure in the small early aggregates remains largely unknown. As experimental evidence suggests that the most toxic species along the aggregation pathway are the small early ones, developing strategies to alleviate disease pathology calls for understanding the structure of polyglutamine peptides in the early stages of aggregation. Here we present a criterion, grounded in available experimental data, that allows for using kinetic stability of dimers to assess if a given polyglutamine conformer can be on the aggregation path. We then demonstrate that this criterion can be assessed using present-day molecular dynamics simulations. We find that although the α-helical conformer of polyglutamine is very stable, dimers of α-helices lack the kinetic stability necessary to support further oligomerization. Dimers of steric zipper, β-nanotube, and β-pseudohelix conformers are also too short-lived to initiate aggregation. The β-hairpin-containing conformers, instead, invariably form very stable dimers when their sidechains are interdigitated. Combining these findings with the implications of recent solid-state NMR data on mature fibrils, we propose a possible pathway for the initial stages of polyglutamine aggregation, in which β-hairpin-containing conformers act as templates for fibril formation.

Insert Received for publication Date and in final form Date.

Corresponding authors: Markus S. Miettinen (email: markus.miettinen@iki.fi, tel: +49 30 838 52226, fax: +49 30 838 5674) and Zoya Ignatova (email: ignatova@uni-potsdam.de, tel: +49 331 977 5130, fax: +49 331 977 5128)

*Current address: IBCP, CNRS UMR 5086, and University Lyon I, 7 Passage du Vercors, 69367, Lyon, France
†Current address: Department of Physics and Astronomy, Clemson University, USA
‡Current address: Biomolecular Dynamics, Institute of Physics, Albert Ludwigs University, Hermann-Herder Strasse 3, D-79104 Freiburg, Germany

0006-3495/08/09/2624/12 $2.00 doi: 10.1529/biophysj.106.090944

Introduction

Protein misfolding and aggregation is connected to many devastating neurodegenerative diseases. One particularly interesting subset of these pathologies comprises the polyglutamine (polyQ) disorders, including Huntington's disease and several ataxias (1). In these dominantly inherited diseases, the aggregating protein contains a polyQ sequence that has expanded beyond a certain threshold (typically between 30 to 40 consecutive glutamines), conferring pathogenicity and triggering the aggregation of the protein in question (1, 2). The sequences flanking the polyQ stretch vary among the proteins, leading to differences in the exact threshold length, age of disease onset, and the course of neurodegeneration (3, 4). However, as the expanded polyQ stretch is the only common feature among the disease-causing polyQ proteins, understanding its structure and properties seems to be key to understanding their shared pathological behavior.

The mature fibrillar aggregates of different polyQ proteins appear to have β-rich secondary structure with a core that has been shown to be dominated by the polyQ stretch (5–7). Using model peptides focused on the polyQ stretch, the principal details of the core structure have emerged: most likely the β-strands run perpendicular to the fibril axis, antiparallel β-sheets form along the axis, and the β-sheets stack such that their side chains interdigitate (8–10). Mounting evidence suggests, however, that these mature aggregates are not toxic enough to be the main culprit of neuronal death (11–19). On the other hand, some small soluble species occurring in the initial stages of aggregation are probably highly toxic (20–27), but here the structural details are largely missing. Revealing the polyQ conformers that occur during the initial stages of aggregation would, therefore, be beneficial for developing strategies that aim to alleviate disease pathology by targeting the toxic species.

To the present time, it has not been experimentally possible to obtain high-resolution structural information on the aggregation-initiating conformation of polyQ peptides. A number of widely different structural models have been proposed. These include the water-filled β-nanotube (based on low-resolution x-ray diffraction on mature fibrils (28)); the dry-core β-pseudohelix (molecular simulations (29, 30)); the β-sheet (mutational analysis (31) and solid-state NMR on fibrils (32)); the β-sheetstack (aggregation kinetics (33)); the steric zipper (first speculated based on a model for another peptide (34), recently supported by solid-state NMR on fibrils (10)); and the α-helix (bioinformatics analysis of interaction partners of polyQ proteins, circular dichroism, and chemical cross-linking (35)). However, the feasibility of the different models has never been systematically compared, possibly due to the lack of criteria for the assessment.

Here we present a criterion to assess the feasibility of different structural models of polyQ to be found on the aggregation path. The criterion is deduced from a mechanistic model regularly used to analyze polyQ aggregation kinetics, and is based on experimental data. We then use this criterion to assess the likelihood of different aggregation pathways via molecular docking calculations and atomistic molecular dynamics (MD) simulations. We find that most of the models proposed in the literature cannot form long-lived dimers, required in the early stages of aggregation. We also show that, among the different models tested, the most stable dimer conformers always contain β-hairpins with interdigitated sidechains, indicating that the formation of this motif could be crucial in the initial stages of polyQ aggregation.

Methods

Nucleated growth polymerization model

As a starting point for our analysis we used the model sketched in Fig. 1. The model was initially proposed based on *in vitro* aggregation kinetics of polyQ peptides (36), and it has since then been regularly applied in this context (for a recent review see Ref. (37)).

The model considers only homogeneous (primary) nucleation, and it excludes any secondary pathways, on which aggregates would spawn new aggregates via processes such as fibril fragmentation (38) or surface-catalyzed nucleation (39). This choice agrees with the experimental finding (36) that the early-time rise in spontaneous aggregation kinetics profiles does not show the exponential signature of a secondary nucleation mechanism, but is polynomial ($\sim t^2$), suggesting primary nucleation to be dominant (40). The finding that seeding turns the sigmoidal profile concave (41) also signals primary nucleation (40).

In the non-aggregating monomer ensemble 'M' (Fig. 1), the model considers polyQ to be (based on circular dichroism (42) and fluorescence correlation spectroscopy (43)) intrinsically disordered and resemble a polymer collapsed in poor solvent. Furthermore, as the mild concentration dependence of the early-time kinetics (of pathological length polyQ, $\mathrm{Q}_{\mathrm{N}>25}$ (33)) translates into a nucleus size 1 in a nucleated polymerization theory analysis, the model considers that 'M' is in pre-equilibrium with the free-energetically most unfavorable state along the aggregation pathway, '1', in which monomers have a particular folded form, capable of triggering aggregation (36). Formation of a dimer '2' is the first step down the free energy landscape; from there on, an on-pathway state 'n' has a higher likelihood to elongate (into 'n+1') than to dissociate (into 'n-1'). Aggregate growth by monomer addition is suggested by the finding that the early polymerization rate is directly proportional to both monomer and aggregate concentrations (40, 44, 45).

Monomeric conformers

We used PyMol (The PyMOL Molecular Graphics System, Version 1.2r3pre, Schrödinger, LLC), VMD (46), and published structures to generate six polyglutamine conformers described in the literature: the steric zipper (10, 34), the β-nanotube (28), the β-pseudohelix (29, 30), the β-sheet (31, 32), the β-sheetstack (33), and the α-helix (35). All peptides consisted of 40 glutamine residues (Q_{40}), with NH_2/COOH-termini. Their stability as monomers has been studied previously (47).

Docking

Docking calculations allow the generation of dimer structures and their ranking according to an estimate of their binding affinity. For each of the six Q_{40} conformers, we docked two identical copies of the peptide on each other using Autodock 4.2 with its default force field parameters (48). A Lamarckian genetic algorithm was used for searching molecular conformations and a grid-based approach was used for energy calculations. The size of the grid was fixed at 0.05 nm. Each docking set comprised 140 copies, and the number of searches in each copy was 25 million. For each set, the 140 docked conformations were clustered based on their mutual RMSD, each group thus representing a binding mode.

First, both monomers were treated as rigid bodies. In order to further optimize the docked conformations, rigid docking was followed by semi-flexible docking. Docked structures from rigid docking were examined and the sidechains at the monomer–monomer interface were made flexible, i.e., the C_α–C_β bonds of side chains were allowed to rotate. If the number of side chains at the interface exceeded ten, they were divided into two groups, and two separate sets of docking calculations were performed making one group rigid and the other flexible. Using semi-flexible docking, structural particularities of the monomer constructs appeared not to prevent representative dimerization of the conformers, but highly compatible (especially for steric zippers and β-sheets) as well as intuitive dimer structures emerged.

Note that as the entropy loss can not be estimated, the docking scores do not represent free energies of binding. However, high scores indicate high dimerization propensity, and allow the selection of probable dimer structures to be used for the kinetic stability analysis in atomistic MD simulations.

Molecular dynamics

To assess the kinetic stability of nine high-scoring dimers obtained via docking, we performed extensive MD simulations.

Two identical sets of atomistic simulations were performed using GROMACS (49) version 4.5.3, one set with the united-atom GROMOS 43a1 (50) and one set with the all-atom CHARMM27 (51, 52) force field. Before starting the simulations, the structures obtained via the docking were relaxed through two energy minimizations (using the steepest descent algorithm) with the respective force fields: first without and then with constraints. Water was then added and, while position-restraining the dimer, relaxed via short MD simulations. In CHARMM27 this was done with 5 000 steps of 0.2 fs followed by 50 000 steps of 2 fs, in GROMOS 43a1 with 25 000 steps of 4 fs. Finally, ten identical copies of each of the 18 systems were given new uncorrelated particle velocities from a Maxwell–Boltzmann distribution at 310 K.

In the GROMOS 43a1 simulations, the simple point charge (SPC) water model (53), heavy hydrogens (54), reaction field electrostatics ($\epsilon_{\mathrm{rf}} = 54$), and a 4 fs time step were used. The van der Waals and Coulomb interactions were cut off at 1.4 nm, and the neighbor lists ($r = 1.4$ nm) updated every step. In the CHARMM27 simulations, the TIP4P water model (55), Particle Mesh Ewald (PME) (56, 57) electrostatics and a 2 fs time step were used. For PME, we used 4^{th}-order interpolation, a 1.3 nm real-space cut-off, a relative error of 10^{-5} in the direct and the reciprocal space, and size-optimized Fast Fourier Transform parameters (grid spacing of roughly 0.12 nm). The neighbor lists ($r = 1.3$ nm) were updated every 10 steps, the van der Waals interactions switched off between 1.0 and 1.2 nm.

All 180 simulations had periodic dodecahedron boundary conditions (initial distance from the dimer atoms to the face of the unit cell ≥ 1.2 nm). Pressure was kept at 1 bar using an isotropically coupled ($\tau = 1.0$ ps) Parrinello–Rahman barostat (58). Temperature was maintained at 310 K using the velocity rescale thermostat (59), separately coupled to the peptides and water ($\tau = 0.1$ ps in GROMOS 43a1 and 1.0 ps in CHARMM27). Covalent bonds were constrained to their equilibrium lengths by (4^{th}-order single-iteration) Parallel Linear Constraint Solver (P-LINCS) (60) in the peptides and SETTLE (61) in water. All 180 simulations were carried out for 100 ns, for a total simulation time of 18 μs.

Results

Lifetime criterion for on-pathway dimers

The mechanistic model that we considered is suggested by kinetic experiments on polyQ peptides (36). In the model (see Fig. 1 and Methods), polyQ aggregation is nucleated by an alternatively-folded monomer (state '1' in Fig. 1), and the formation of an on-pathway dimer ('2') is the first step downhill in the free energy landscape (36, 37, 62).

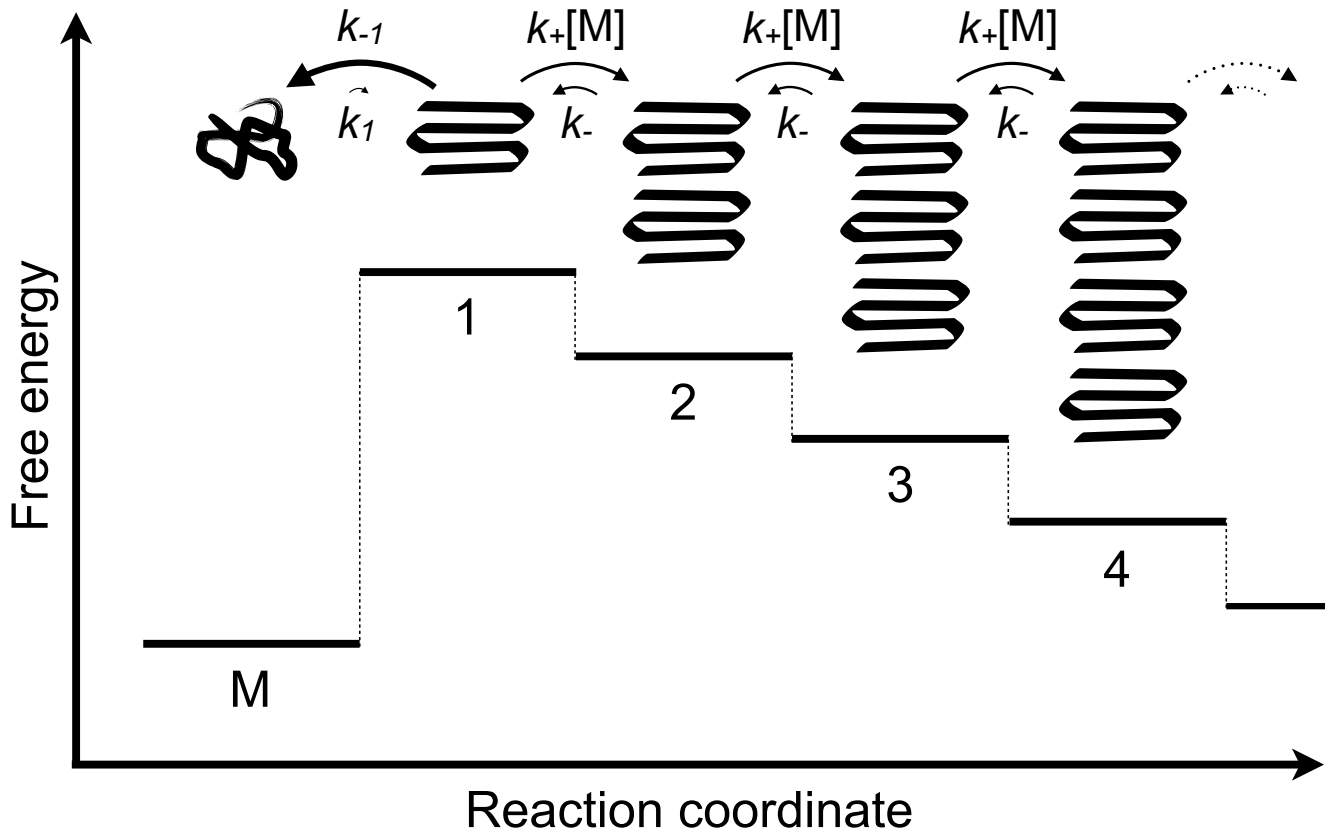

Figure 1: Initiation of polyQ aggregation according to the nucleated growth polymerization model suggested by Wetzel *et al.* (36, 37, 62). The model considers that the non-aggregating monomer ensemble 'M' is in pre-equilibrium with the free-energetically most unfavorable state along the aggregation pathway, '1', in which monomers are found in a conformation capable of initiating aggregation (36). For pathological-length polyQ, the population ratio between the states 'M' and '1' is estimated to be of the order of billion-to-one (63). Notably, due to asymmetric exit-rates ($k_{-1} > k_+[\mathrm{M}]$, indicated by the length and thickness of arrows), a peptide in state '1' would still be much more likely to go to state 'M' than to '2' (37). From state 'n'$\geq$2 the state 'n+1' is more likely than 'n–1'. As the monomer concentration [M] is initially effectively constant, we depict all the reactions as first-order, with the (second order) growth reaction taking place with a pseudo-first-order reaction rate $k_+[\mathrm{M}]$.

Notably, the on-pathway dimer has a higher likelihood to elongate than to disintegrate (37), which gives a means to assess if a given dimer structure can be on the aggregation path: The disintegration time of the on-pathway dimer will exceed the time required for its elongation into the on-pathway trimer ('3').

In fact, for the diffusion along the reaction coordinate to drive the system towards the fibrillar state, for all on-pathway states 'n' ≥ 2 the probability to enter the state 'n+1' must exceed 50%. That is, going from 'n' to 'n+1' must be more likely than exiting 'n' through any disintegrative route. In terms of rate constants, this condition reads as $k_+[\mathrm{M}] > k_- + k_{-n}$. Here $k_+[\mathrm{M}]$ and k_- are as shown in Fig. 1; k_{-n} is the exit rate to any disintegrated state other than 'n-1', which is considered to be vanishingly small for on-pathway states, and is thus not drawn in Fig. 1.

Thus, a necessary condition for a given dimer structure to be on the aggregation pathway is that its characteristic disintegration time $\tau_{\mathrm{dis}} = 1/(k_- + k_{-2})$, in other words the time over which the dimer structure stays unchanged, exceeds the

characteristic time $\tau_{\mathrm{fwd}} = 1/k_+[\mathrm{M}]$ needed for the elongation step to occur. Hence, for aggregation to proceed, the dimer must fulfill the following stability condition:

$$\tau_{\mathrm{dis}} > \tau_{\mathrm{fwd}} = \frac{1}{k_+[\mathrm{M}]} = \frac{1}{(2 \times 10^4\ {}^1\!/_{\mathrm{s}}\ {}^1\!/_{\mathrm{M}}) \times (50 \times 10^{-6}\ \mathrm{M})} = 1\ \mathrm{s}. \quad (1)$$

Here we used the conservative estimates $k_+ = 2 \times 10^4\ {}^1\!/_{\mathrm{s}}\ {}^1\!/_{\mathrm{M}}$ and $[\mathrm{M}] = 50\ \mu\mathrm{M}$ (the elongation constant k_+ has been measured to be $1.14 \times 10^4\ {}^1\!/_{\mathrm{s}}\ {}^1\!/_{\mathrm{M}}$ for $\mathrm{K_2Q_{47}K_2}$ (63), and typical initial concentrations in experiments are 5 to 200 μM, see for example Refs. (33, 36, 63)).

Hence, if the average lifetime of a dimer is not at least one second, the dimer in question cannot be on the aggregation pathway. In particular, for a given dimer structure to be on-pathway, it must show extreme kinetic stability on the time scale of hundreds of nanoseconds that is typical for MD simulations. For the on-pathway dimer, the likelihood of disintegration during 100 ns is: $1 - \exp(-100 \times 10^{-9}) \approx 10^{-7}$, that is, 1 in 10 million dimers is expected to disintegrate during 100 ns. The kinetic stability of peptide dimers is therefore a useful criterion for assessing candidate structures for the initial stages of polyQ aggregation.

A defining feature of the lifetime criterion is that it is, per construction, a tool of exclusion, not inclusion. It can eliminate unfeasible structures, but never fully prove that a given structure is on-pathway. This logic holds independent of the simulation length; even stability beyond the time limit of Eq. (1) does not provide an exact proof that a structure is on-pathway—only that it could be. With confidence, however, all structures failing to reach this time limit can be removed from the list of possible on-pathway candidates.

Construction of polyQ dimers with peptide–peptide docking

We generated dimers comprising two $\mathrm{Q_{40}}$-peptides using semi-rigid peptide–peptide docking calculations on six different conformers: β-sheet, β-sheetstack, steric zipper, β-nanotube, β-pseudohelix and α-helix. When using the docking approach, one makes the implicit assumption that no major monomer restructuring occurs upon dimerization; here this assumption appears plausible as the highest free energy state is known to be a structured monomer (Fig. 1). The initial monomer structures for the conformers were the same as in our previous study (47). The docking scores acquired from the calculations provided qualitative information on the stability of dimers (under the assumption of static conformers) and allowed for a rough comparison of their elongation potentials.

The highest docking score (49; given in -kcal/mol by Autodock (48)) occurred for two exactly aligned steric zipper peptides (Fig. 2). The high score reflected the large number of inter-peptide hydrogen bonds, indicating that this conformer possesses a high elongation potential along this mode of binding. A high score (30) was also obtained when one of the monomers was rotated 180° in the plane of its backbone. For this orientation, however, the semi-rigid docking did not result in a perfect alignment of the β-strands and no β-sheets were formed (Fig. 2).

The second highest score (35) was obtained for a β-sheet dimer that had the β-sheets stacked on top of one another, with their sidechains interdigitated (Fig. 2). No inter-peptide hydrogen bonding occurred, and the peptide–peptide interactions were mostly dispersion interactions, as the tight-fitting interdigitation provided many close contacts between the sidechains.

The high-scoring β-sheet dimer was similar to the two high-scoring configurations found for the β-sheetstack dimer (23 and 27; Fig. 2). As the sidechains were already interdigitated in the β-sheetstack monomer, the dimerization took place by establishing backbone–backbone and sidechain–sidechain hydrogen bonds between the two polyQ peptides.

The tube-like conformers (β-nanotube and β-pseudohelix) were barely distinguishable in their scores (21 and 19), reflecting the high similarity in their mode of binding (along the tube axis, see Fig. 2). Interestingly, the polyQ in α-helical conformation showed the lowest docking scores (13 for the parallel and 10 for the antiparallel orientation), indicating a low elongation potential.

Assessment of dimer kinetic stability with MD simulations

The dimers obtained for each conformer via docking gave good initial configurations that were used for studying the kinetic stability of dimers by atomistic MD simulations. For each of the nine high-scoring dimeric structures (Fig. 2) 10+10 independent MD simulations (180 simulations in total) of 100 ns were performed using two different force fields, CHARMM27 (51, 52) and GROMOS 43a1 (50), with an explicit solvent. We emphasize that as different MD force fields can differ in their ability to describe some features of peptides (64–66), we repeated all our MD simulations with two different atomistic force fields. This gives us a good control over possible systematic errors and allows verifying the significance of our observations.

The kinetic stability of the conformers was estimated by monitoring their lifetimes, obtained by visual inspection of the trajectories and analysis of the root mean squared deviation (RMSD) of dimer backbone atom distances (signaling conformational changes of the dimer), and the peptide–peptide center of mass distance (signaling separation of the monomers). Details of the analysis are available in the Supporting Information.

Comparison of the kinetic stabilities revealed that the β-hairpin-containing dimers (β-sheet and β-sheetstack dimers) displayed unwavering stability, maintaining their secondary structure (Figs. S1 and S3 in the Supporting Material) and a short inter-molecular distance (Fig. S2) throughout the simulation (100 ns) in all the 60 replicas (Fig. 3).

The α-helix dimers also showed rather high stability, but disintegration events occurred in three of the 40 replicas: twice via monomer separation, and once through a structural collapse of the dimer (Fig. S4). Notably, the latter was the only replica in which either of the α-helix monomers lost its conformation.

Dimers of the other three conformers (β-nanotube, β-pseudohelix, and steric zipper) showed low stability, with all β-nanotube replicas and all but one steric zipper replica disintegrating before 100 ns (Fig. 3). The β-nanotube was the only conformer in addition to the α-helix that experienced a separation of monomers (Fig. S5).

Discussion

In this study, we pointed out that according to a mechanistic model regularly used to analyze polyQ aggregation kinetics (Fig. 1), the lifetime of an on-pathway polyQ dimer must exceed by more than six orders of magnitude the typical (100 ns)

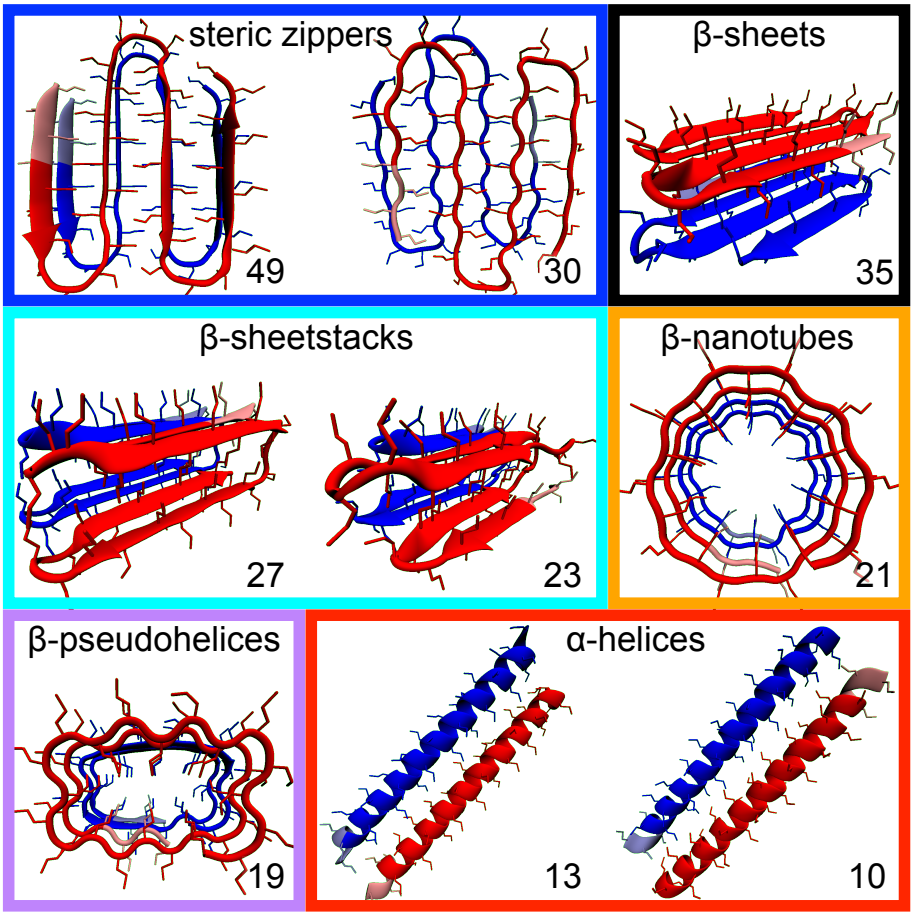

Figure 2: The highest-scoring polyQ dimer structures obtained with peptide–peptide docking are shown as snapshots. One monomer is colored red, the other blue; three N-terminal residues are represented with a lighter shade of the same colors. The numbers indicate the docking scores (given by Autodock in -kcal/mol) of the modes of binding. The color-coding of the frames corresponds to that of the lines in Fig. 3.

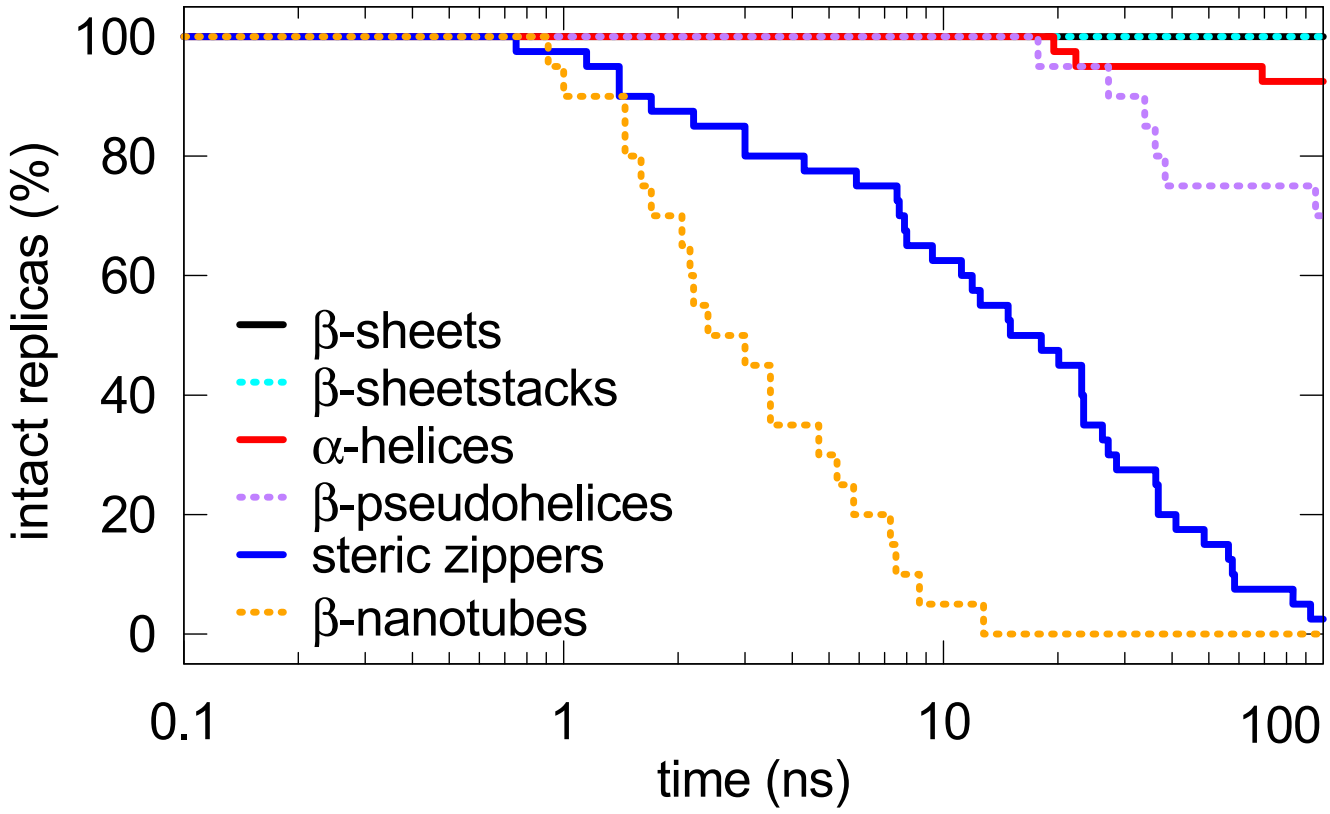

Figure 3: The percentage of intact dimers (whose monomers retain their initial conformation and remain associated) as a function of MD simulation time. All replicas are grouped under the conformer of the monomer, irrespective of the relative orientation of the peptides and the force field used. The color-coding is as in Fig. 2.

time scale of present-day MD simulations. Therefore, should an on-pathway dimer be simulated via MD, it should demonstrate extreme kinetic stability. We then created a set of nine polyQ dimers (of six different conformers, see Fig. 2) and performed extensive (180×100 ns) MD simulations on them. We found that the α-helical, β-nanotube, β-pseudohelix and steric zipper dimers were not stable enough to be on the polyQ aggregation pathway. Instead, the extreme stability of dimers comprising β-hairpins stacked such that their side chains interdigitate (the β-sheet and β-sheetstack dimers) indicated that the on–pathway dimers could include this motive.

Characteristic lifetime

Based on the initial growth rate of on-pathway states, $k_+[\mathrm{M}]$, we deduced that the characteristic lifetime of an on-pathway dimer must exceed one second (Eq. (1)). This estimate is still rather conservative, as can be gauged from the rate of the dissociation reaction, k_-, at the long time limit. When fibril formation reaches equilibrium, it holds that $k_- = k_+[\mathrm{M}]_\mathrm{c}$. Here $[\mathrm{M}]_\mathrm{c}$ is the characteristic final monomer concentration; it is equivalent to the critical initial monomer concentration, below which spontaneous fibril formation does not occur. The value of $[\mathrm{M}]_\mathrm{c}$ has been measured experimentally, and is known to decrease as polyQ length increases: $[\mathrm{M}]_\mathrm{c} \approx 30\ \mu$M for $\mathrm{K_2Q_{15}K_2}$ (41), $\approx 3\ \mu$M for $\mathrm{K_2Q_{23}K_2}$ (33), $\leq 1\ \mu$M for $\mathrm{K_2Q_{28}K_2}$ (67), and is still less for longer polyQ sequences (37, 41). Using the estimates $[\mathrm{M}]_\mathrm{c} = 1\ \mu$M and $k_+ = 1.14 \times 10^4\ {}^1\!/_\mathrm{s}\ {}^1\!/_\mathrm{M}$ (still conservative for $\mathrm{Q_{40}}$) gives $k_- = 1.14 \times 10^{-2}\ {}^1\!/_\mathrm{s}$ and a characteristic lifetime for on-pathway states $1/k_- \approx 90$ s. Should a species be able to trigger neuronal death (68, 69), this could be enough time to execute the toxic mission.

Kinetic stabilities of dimers

For the on-pathway dimer, no disintegration events should occur during the 100 ns MD simulations we performed here. Of the structures studied, only the β-sheet and β-sheetstack dimers achieved this (Fig. 3).

Dimers of Q_{40} were built by docking monomeric structures proposed in the literature. We had previously explored their kinetic stabilities as monomers, and shown that both α-helical and β-hairpin-containing monomers have average lifetimes exceeding 100 ns (47). With the exception of the α-helix, all the conformers gained kinetic stability upon dimerization.

The α-helical dimers did not demonstrate (Fig. 3) the extreme kinetic stability required for the on-pathway dimer (Eq. (1)). In fact, as predicted by the low docking scores (Fig. 2), the α-helical monomers did not bind to one another very strongly, but in 5% of the MD simulations the α-helix dimers were observed breaking into monomers. As expected based on their robustness as monomers (47), the monomers retained their α-helical conformations in these events. Thus, although the polyQ stretch may populate the α-helical conformation as a monomer (35), the elongation into fibrils would only be feasible after a conformational conversion (70). We conclude that the α-helical assemblies are most likely off-pathway with regards to polyQ aggregation.

The low kinetic stabilities observed here for the β-nanotube and the β-pseudohelix are consistent with other atomistic MD studies showing that (based on backbone RMSDs) dimers of tube-like conformers have short (10–50 ns) lifetimes (71, 72).

The excellent compatibility of the steric zippers (signaled by their high docking scores in Fig. 2) led to a considerable stabilization upon dimerization: The average lifetime increased by two orders of magnitude from the sub-nanosecond times reported for monomers (47). Interestingly, however, this stabilization was still not enough to make the dimers last beyond 100 ns (Fig. 3). In contrast, the β-hairpin-containing dimers (i.e., the β-sheet and β-sheetstack) showed very high kinetic stability: none of the β-hairpin-containing dimers broke during the entire simulation time (60×0.1 μs). The stabilizing effect of β-hairpins has been demonstrated previously, as a dimer created by joining two Q_{15} hairpins in the same plane, forming a 4-strand β-sheet, was not stable over 10 ns (73), but a monomeric (Q_{40}) 4-strand β-sheet had an average lifetime exceeding 100 ns (47). Our simulations are consistent with these results and with the high stabilities reported for large collections of extended β-strands (Q_6 and Q_{15}) organized into interdigitated β-sheets (74). Taken together, all these findings indicate that the β-hairpin motif alone is not sufficient to obtain an extremely stable structure, but that sidechain interdigitation, characteristic of the steric zipper conformer, is also required. It appears that 3–4 strands in the β-sheet-direction and 2 strands in the steric-zipper-direction is enough for creating a highly stable system. The high stability is particularly interesting in the light of reports that indicate the very toxic soluble species to contain β-hairpins (23, 75, 76).

Possible pathway

It is noteworthy that the three conformers we found to have the highest docking scores (steric zipper, β-sheet and β-sheetstack) only differ in their turn regions (Fig. 2). In the β-sheet the turns are sharp hairpins, in the steric zipper rather gentle arches (77). The β-sheetstack includes both turn types, and thus demonstrates the compatibility of the β-sheet and steric zipper conformers. Notably, all three could, in principle, fit the tight packing of β-strands found in the final fibrils.

The steric-zipper-based fibril was recently supported by Schneider *et al.* (10). They report their solid-state NMR results to be most compatible with peptides in a steric-zipper-like conformation, and not with a conformation containing β-hairpins. The high docking scores we obtained for the steric zipper (Fig. 2) are consistent with the results of Schneider *et al.* However, as is evident from the lack on kinetic stability of the steric zipper dimer (Fig. 3), a docking event of this kind would only be feasible provided that a robust, steric-zipper-compatible fibril already exists.

Support for the β-hairpin-containing fibrils, then, came from Kar *et al.* (32). They used solid-state NMR to show that certain β-hairpin-enhancing mutations in polyQ peptides do not change the resulting fibril structure. The formation rates of fibrils, however, increase greatly. They thus argue that β-hairpin-containing structures are the most likely ones to be found in the nucleus and in the final fibril. Our main finding that only the β-hairpin-containing dimers are long-lived enough to be on-pathway (Fig. 3) is consistent with the results of Kar *et al.*. However, the fibril elongation can evidently not occur via β-sheet stacking (which was the arrangement found by the docking algorithm for the β-sheet dimer, see Fig. 2), as the fibril axis should be aligned with (and not perpendicular to) the plane of the β-sheets forming it (9, 78).

In short, it seems that in the nucleation event the β-hairpin-containing conformers are required (32), whereas the steric zippers better fit the final fibril (10). Based on our findings, we suggest that a possible explanation to this apparent contradiction lies in the inherent compatibility of the two conformers. As we demonstrated, the steric zipper dimers are too unstable to be on the aggregation path. In the initial stages of aggregation the β-hairpin motif thus appears crucial. We also demonstrated that for unwavering stability the sidechains of the β-hairpins should be interdigitated. This, notably, creates a surface that is compatible with the steric zipper conformer. We therefore suggest that in the initial stages β-hairpin-containing peptides come together, creating a robust surface, on which further peptides then deposit themselves in the steric zipper conformation.

This pathway agrees with both the finding that the final fibrils contain predominantly steric zippers (10), and that enhancing the ability of β-hairpin formation will enhance the rate of fibril formation (32). Furthermore, it explains the finding of Kar *et al.* that while the nucleation of fibril formation is greatly facilitated by the β-hairpin-enhancing insertion, the elongation phase is actually somewhat retarded by it (32). Evidently, preference for β-hairpins would speed up the initial steps on our suggested path, but slow down the later steps, in which arch-like turns, characteristic of the steric zipper conformer, need to form.

The possible medical implications of this pathway would be related to the relatively benign effects of the mature aggregates (11–19) versus the high toxicity of early soluble species (20–27). Therapeutic strategies could be designed to encourage steric-zipper-like conformers (and thus aggregate maturation) while discouraging β-hairpin formation (and thus aggregate emergence).

Acknowledgments

We thank Drs. Luciana Esposito, Pawel Sikorski and David Zanuy for kindly sharing their structural models, and Cristiano L. Dias, Yann von Hansen and Christoph Röthlein for inspiring discussions. M.S.M. acknowledges support from the Finnish Foundation for Technology Promotion (TES), the HPC-Europa2 visitor project (#228398, supported by the European Commission—Capacities Area—Research Infrastructures), the European Molecular Biology Organization fellowship (EMBO ALTF 1251-2010), and Volkswagen Foundation (86110). This work was supported by the Deutsche Forschungsgemeinschaft (IG 73/8-1) grant to Z.I.

SUPPLEMENTARY MATERIAL

An online supplement to this article can be found by visiting BJ Online at http://www.biophysj.org.

References

1. Orr, H. T., and H. Y. Zoghbi. 2007. Trinucleotide Repeat Disorders. *Annu. Rev. Neurosci.* 30:576–621.
2. Scherzinger, E., A. Sittler, K. Schweiger, V. Heiser, R. Lurz, R. Hasenbank, G. P. Bates, H. Lehrach, and E. E. Wanker. 1999. Self-assembly of polyglutamine-containing huntingtin fragments into amyloid-like fibrils: Implications for Huntington's disease pathology. *Proc. Natl. Acad. Sci. U.S.A.* 96:4604–4609.
3. Hands, S. L., and A. Wyttenbach. 2010. Neurotoxic protein oligomerisation associated with polyglutamine diseases. *Acta Neuropathol.* 120:419–437.
4. Bauer, P. O., and N. Nukina. 2009. The pathogenic mechanisms of polyglutamine diseases and current therapeutic strategies. *J. Neurochem.* 110:1737–1765.
5. Scherzinger, E., R. Lurz, M. Turmaine, L. Mangiarini, B. Hollenbach, R. Hasenbank, G. P. Bates, S. W. Davies, H. Lehrach, and E. E. Wanker. 1997. Huntingtin-Encoded Polyglutamine Expansions Form Amyloid-like Protein Aggregates In Vitro and In Vivo. *Cell* 90:549–558.
6. Bevivino, A. E., and P. J. Loll. 2001. An expanded glutamine repeat destabilizes native ataxin-3 structure and mediates formation of parallel β-fibrils. *Proc. Natl. Acad. Sci. U.S.A.* 98:11955–11960.
7. Hinz, J., L. Lehnhardt, S. Zakrzewski, G. Zhang, and Z. Ignatova. 2012. Polyglutamine Expansion Alters the Dynamics and Molecular Architecture of Aggregates in Dentatorubropallidoluysian Atrophy. *J. Biol. Chem.* 287:2068–2078.
8. Perutz, M. F., T. Johnson, M. Suzuki, and J. T. Finch. 1994. Glutamine repeats as polar zippers: Their possible role in inherited neurodegenerative diseases. *Proc. Natl. Acad. Sci. U.S.A.* 91:5355–5358.
9. Sikorski, P., and E. Atkins. 2005. New Model for Crystalline Polyglutamine Assemblies and Their Connection with Amyloid Fibrils. *Biomacromolecules* 6:425–432.
10. Schneider, R., M. C. Schumacher, H. Mueller, D. Nand, V. Klaukien, H. Heise, D. Riedel, G. Wolf, E. Behrmann, S. Raunser, R. Seidel, M. Engelhard, and M. Baldus. 2011. Structural Characterization of Polyglutamine Fibrils by Solid-State NMR Spectroscopy. *J. Mol. Biol.* 412:121–136.
11. Klement, I. A., P. J. Skinner, M. D. Kaytor, H. Yi, S. M. Hersch, H. B. Clark, H. Y. Zoghbi, and H. T. Orr. 1998. Ataxin-1 Nuclear Localization and Aggregation: Role in Polyglutamine-Induced Disease in SCA1 Transgenic Mice. *Cell* 95:41–53.
12. Saudou, F., S. Finkbeiner, D. Devys, and M. E. Greenberg. 1998. Huntingtin Acts in the Nucleus to Induce Apoptosis but Death Does Not Correlate with the Formation of Intranuclear Inclusions. *Cell* 95:55–66.
13. Yoshizawa, T., H. Yoshida, and S. Shoji. 2001. Differential susceptibility of cultured cell lines to aggregate formation and cell death produced by the truncated Machado–Joseph disease gene product with an expanded polyglutamine stretch. *Brain Res. Bull.* 56:349–352.
14. Arrasate, M., S. Mitra, E. S. Schweitzer, M. R. Segal, and S. Finkbeiner. 2004. Inclusion body formation reduces levels of mutant huntingtin and the risk of neuronal death. *Nature* 431:805–810.

15. Bowman, A. B., S.-Y. Yoo, N. P. Dantuma, and H. Y. Zoghbi. 2005. Neuronal dysfunction in a polyglutamine disease model occurs in the absence of ubiquitin–proteasome system impairment and inversely correlates with the degree of nuclear inclusion formation. *Hum. Mol. Genet.* 14:679–691.
16. Slow, E. J., R. K. Graham, A. P. Osmand, R. S. Devon, G. Lu, Y. Deng, J. Pearson, K. Vaid, N. Bissada, R. Wetzel, B. R. Leavitt, and M. R. Hayden. 2005. Absence of behavioral abnormalities and neurodegeneration *in vivo* despite widespread neuronal huntingtin inclusions. *Proc. Natl. Acad. Sci. U.S.A.* 102:11402–11407.
17. Rüb, U., R. A. I. De Vos, E. R. Brunt, T. Sebestény, L. Schöls, G. Auburger, J. Bohl, E. Ghebremedhin, K. Gierga, K. Seidel, W. Den Dunnen, H. Heinsen, H. Paulson, and T. Deller. 2006. Spinocerebellar Ataxia Type 3 (SCA3): Thalamic Neurodegeneration Occurs Independently from Thalamic Ataxin-3 Immunopositive Neuronal Intranuclear Inclusions. *Brain Pathol.* 16:218–227.
18. Miller, J., M. Arrasate, B. A. Shaby, S. Mitra, E. Masliah, and S. Finkbeiner. 2010. Quantitative Relationships between Huntingtin Levels, Polyglutamine Length, Inclusion Body Formation, and Neuronal Death Provide Novel Insight into Huntington's Disease Molecular Pathogenesis. *J. Neurosci.* 30:10541–10550.
19. Zuccato, C., M. Valenza, and E. Cattaneo. 2010. Molecular Mechanisms and Potential Therapeutical Targets in Huntington's Disease. *Physiol. Rev.* 90:905–981.
20. Watase, K., E. J. Weeber, B. Xu, B. Antalffy, L. Yuva-Paylor, K. Hashimoto, M. Kano, R. Atkinson, Y. Sun, D. L. Armstrong, J. D. Sweatt, H. T. Orr, R. Paylor, and H. Y. Zoghbi. 2002. A Long CAG Repeat in the Mouse Sca1 Locus Replicates SCA1 Features and Reveals the Impact of Protein Solubility on Selective Neurodegeneration. *Neuron* 34:905–919.
21. Sanchez, I., C. Mahlke, and J. Yuan. 2003. Pivotal role of oligomerization in expanded polyglutamine neurodegenerative disorders. *Nature* 421:373–379.
22. Ross, C. A., and M. A. Poirier. 2005. What is the role of protein aggregation in neurodegeneration? *Nat. Rev. Mol. Cell Biol.* 6:891–898.
23. Nagai, Y., T. Inui, H. A. Popiel, N. Fujikake, K. Hasegawa, Y. Urade, Y. Goto, H. Naiki, and T. Toda. 2007. A toxic monomeric conformer of the polyglutamine protein. *Nat. Struct. Mol. Biol.* 14:332–340.
24. Li, M., E. S. Chevalier-Larsen, D. E. Merry, and M. I. Diamond. 2007. Soluble Androgen Receptor Oligomers Underlie Pathology in a Mouse Model of Spinobulbar Muscular Atrophy. *J. Biol. Chem.* 282:3157–3164.
25. Takahashi, T., S. Kikuchi, S. Katada, Y. Nagai, M. Nishizawa, and O. Onodera. 2008. Soluble polyglutamine oligomers formed prior to inclusion body formation are cytotoxic. *Hum. Mol. Genet.* 17:345–356.
26. Miller, J., M. Arrasate, E. Brooks, C. P. Libeu, J. Legleiter, D. Hatters, J. Curtis, K. Cheung, P. Krishnan, S. Mitra, K. Widjaja, B. A. Shaby, G. P. Lotz, Y. Newhouse, E. J. Mitchell, A. Osmand, M. Gray, V. Thulasiramin, F. Saudou, M. Segal, X. W. Yang, E. Masliah, L. M. Thompson, P. J. Muchowski, K. H. Weisgraber, and S. Finkbeiner. 2011. Identifying polyglutamine protein species *in situ* that best predict neurodegeneration. *Nat. Chem. Biol.* 7:925–934.
27. Zhang, Q. C., T.-l. Yeh, A. Leyva, L. G. Frank, J. Miller, Y. E. Kim, R. Langen, S. Finkbeiner, M. L. Amzel, C. A. Ross, and M. A. Poirier. 2011. A Compact β Model of huntingtin Toxicity. *J. Biol. Chem.* 286:8188–8196.
28. Perutz, M. F., J. T. Finch, J. Berriman, and A. Lesk. 2002. Amyloid fibers are water-filled nanotubes. *Proc. Natl. Acad. Sci. U.S.A.* 99:5591–5595.
29. Khare, S. D., F. Ding, K. N. Gwanmesia, and N. V. Dokholyan. 2005. Molecular origin of polyglutamine aggregation in neurodegenerative diseases. *PLoS Comput. Biol.* 1:230–235.
30. Zanuy, D., K. Gunasekaran, A. M. Lesk, and R. Nussinov. 2006. Computational study of the fibril organization of polyglutamine repeats reveals a common motif identified in β-helices. *J. Mol. Biol.* 358:330–345.
31. Thakur, A. K., and R. Wetzel. 2002. Mutational analysis of the structural organization of polyglutamine aggregates. *Proc. Natl. Acad. Sci. U.S.A.* 99:17014–17019.
32. Kar, K., C. L. Hoop, K. W. Drombosky, M. A. Baker, R. Kodali, I. Arduini, P. C. A. van der Wel, W. S. Horne, and R. Wetzel. 2013. β-hairpin-mediated nucleation of polyglutamine amyloid formation. *J. Mol. Biol.* 425:1183–1197.
33. Kar, K., M. Jayaraman, B. Sahoo, R. Kodali, and R. Wetzel. 2011. Critical nucleus size for disease-related polyglutamine aggregation is repeat-length dependent. *Nat. Struct. Mol. Biol.* 18:328–336.
34. Kajava, A. V., U. Baxa, R. B. Wickner, and A. C. Steven. 2004. A model for Ure2p prion filaments and other amyloids: The parallel superpleated β-structure. *Proc. Natl. Acad. Sci. U.S.A.* 101:7885–7890.
35. Fiumara, F., L. Fioriti, E. R. Kandel, and W. A. Hendrickson. 2010. Essential role of coiled coils for aggregation and activity of Q/N-rich prions and PolyQ proteins. *Cell* 143:1121–1135.
36. Chen, S., F. A. Ferrone, and R. Wetzel. 2002. Huntington's disease age-of-onset linked to polyglutamine aggregation nucleation. *Proc. Natl. Acad. Sci. U.S.A.* 99:11884–11889.
37. Wetzel, R. 2012. Physical Chemistry of Polyglutamine: Intriguing Tales of a Monotonous Sequence. *J. Mol. Biol.* 421:466–490.
38. Wegner, A. 1982. Spontaneous fragmentation of actin filaments in physiological conditions. *Nature* 296:266–267.
39. Ferrone, F. A., J. Hofrichter, H. R. Sunshine, and W. A. Eaton. 1980. Kinetic studies on photolysis-induced gelation of sickle cell hemoglobin suggest a new mechanism. *Biophys. J.* 32:361–380.
40. Cohen, S. I. A., M. Vendruscolo, C. M. Dobson, and T. P. J. Knowles. 2012. From macroscopic measurements to microscopic mechanisms of protein aggregation. *J. Mol. Biol.* 421:160–171.
41. Chen, S., V. Berthelier, W. Yang, and R. Wetzel. 2001. Polyglutamine aggregation behavior *in vitro* supports a recruitment mechanism of cytotoxicity. *J. Mol. Biol.* 311:173–182.
42. Altschuler, E. L., N. V. Hud, J. A. Mazrimas, and B. Rupp. 1997. Random coil conformation for extended polyglutamine stretches in

aqueous soluble monomeric peptides. *J. Pept. Res.* 50:73–75.
43. Crick, S. L., M. Jayaraman, C. Frieden, R. Wetzel, and R. V. Pappu. 2006. Fluorescence correlation spectroscopy shows that monomeric polyglutamine molecules form collapsed structures in aqueous solutions. *Proc. Natl. Acad. Sci. U.S.A.* 103:16764–16769.
44. Berthelier, V., J. B. Hamilton, S. Chen, and R. Wetzel. 2001. A Microtiter Plate Assay for Polyglutamine Aggregate Extension. *Anal. Biochem.* 295:227–236.
45. Collins, S. R., A. Douglass, R. D. Vale, and J. S. Weissman. 2004. Mechanism of Prion Propagation: Amyloid Growth Occurs by Monomer Addition. *PLoS Biol.* 2:e321.
46. Humphrey, W., A. Dalke, and K. Schulten. 1996. VMD – Visual Molecular Dynamics. *J. Mol. Graph.* 14:33–38.
47. Miettinen, M. S., V. Knecht, L. Monticelli, and Z. Ignatova. 2012. Assessing Polyglutamine Conformation in the Nucleating Event by Molecular Dynamics Simulations. *J. Phys. Chem. B* 116:10259–10265.
48. Morris, G. M., R. Huey, W. Lindstrom, M. F. Sanner, R. K. Belew, D. S. Goodsell, and A. J. Olson. 2009. AutoDock4 and AutoDockTools4: Automated Docking with Selective Receptor Flexibility. *J. Comput. Chem.* 30:2785–2791.
49. Hess, B., C. Kutzner, D. van der Spoel, and E. Lindahl. 2008. GROMACS 4: Algorithms for Highly Efficient, Load-Balanced, and Scalable Molecular Simulation. *J. Chem. Theory Comput.* 4:435–447.
50. Schuler, L. D., X. Daura, and W. F. van Gunsteren. 2001. An Improved GROMOS96 Force Field for Aliphatic Hydrocarbons in the Condensed Phase. *J. Comput. Chem.* 22:1205–1218.
51. Mackerell, A. D., Jr., M. Feig, and C. L. Brooks, 3^{rd}. 2004. Extending the treatment of backbone energetics in protein force fields: Limitations of gas-phase quantum mechanics in reproducing protein conformational distributions in molecular dynamics simulations. *J. Comput. Chem.* 25:1400–1415.
52. Bjelkmar, P., P. Larsson, M. A. Cuendet, B. Hess, and E. Lindahl. 2010. Implementation of the CHARMM Force Field in GROMACS: Analysis of Protein Stability Effects from Correction Maps, Virtual Interaction Sites, and Water Models. *J. Chem. Theory Comput.* 6:459–466.
53. Berendsen, H. J. C., J. P. M. Postma, W. F. van Gunsteren, and J. Hermans. 1981. Interaction models for water in relation to protein hydration. *In* B. Pullman, editor, Intermolecular Forces, Reidel, Dordrecht. 331–342.
54. Feenstra, K. A., B. Hess, and H. J. C. Berendsen. 1999. Improving Efficiency of Large Time-Scale Molecular Dynamics Simulations of Hydrogen-Rich Systems. *J. Comput. Chem.* 20:786–798.
55. Jorgensen, W. L., J. Chandrasekhar, J. D. Madura, R. W. Impey, and M. L. Klein. 1983. Comparison of simple potential functions for simulating liquid water. *J. Chem. Phys.* 79:926–935.
56. Darden, T., D. York, and L. Pedersen. 1993. Particle mesh Ewald: An $N \cdot \log(N)$ method for Ewald sums in large systems. *J. Chem. Phys.* 98:10089–10092.
57. Essman, U., L. Perela, M. L. Berkowitz, H. L. T. Darden, and L. G. Pedersen. 1995. A smooth particle mesh Ewald method. *J. Chem. Phys.* 103:8577–8592.
58. Parrinello, M., and A. Rahman. 1981. Polymorphic transitions in single crystals: A new molecular dynamics method. *J. Appl. Phys.* 52:7182–7190.
59. Bussi, G., D. Donadio, and M. Parrinello. 2007. Canonical sampling through velocity rescaling. *J. Chem. Phys.* 126:014101.
60. Hess, B. 2008. P-LINCS: A Parallel Linear Constraint Solver for Molecular Simulation. *J. Chem. Theory Comput.* 4:116–122.
61. Miyamoto, S., and P. A. Kollman. 1992. SETTLE: An analytical version of the SHAKE and RATTLE algorithms for rigid water models. *J. Comput. Chem.* 13:952–962.
62. Wetzel, R. 2006. Kinetics and Thermodynamics of Amyloid Fibril Assembly. *Acc. Chem. Res.* 39:671–679.
63. Bhattacharyya, A. M., A. K. Thakur, and R. Wetzel. 2005. Polyglutamine aggregation nucleation: Thermodynamics of a highly unfavorable protein folding reaction. *Proc. Natl. Acad. Sci. U.S.A.* 102:15400–15405.
64. Lange, O. F., D. van der Spoel, and B. L. de Groot. 2010. Scrutinizing Molecular Mechanics Force Fields on the Submicrosecond Timescale with NMR Data. *Biophys. J.* 99:647–655.
65. Cino, E. A., W.-Y. Choy, and M. Karttunen. 2012. Comparison of Secondary Structure Formation Using 10 Different Force Fields in Microsecond Molecular Dynamics Simulations. *J. Chem. Theory Comput.* 8:2725–2740.
66. Lindorff-Larsen, K., P. Maragakis, S. Piana, M. P. Eastwood, R. O. Dror, and D. E. Shaw. 2012. Systematic Validation of Protein Force Fields against Experimental Data. *PLoS ONE* 7:e32131.
67. Chen, S., V. Berthelier, J. B. Hamilton, B. O'Nuallai, and R. Wetzel. 2002. Amyloid-like Features of Polyglutamine Aggregates and Their Assembly Kinetics. *Biochemistry* 41:7391–7399.
68. Clarke, G., R. A. Collins, B. R. Leavitt, D. F. Andrews, M. R. Hayden, C. J. Lumsden, and R. R. McInnes. 2000. A one-hit model of cell death in inherited neuronal degenerations. *Nature* 406:195–199.
69. Colby, D. W., J. P. Cassady, G. C. Lin, V. M. Ingram, and K. D. Wittrup. 2006. Stochastic kinetics of intracellular huntingtin aggregate formation. *Nat. Chem. Biol.* 2:319–323.
70. Liebman, S. W., and S. C. Meredith. 2010. Protein folding: Sticky N17 speeds huntingtin pile-up. *Nat. Chem. Biol.* 6:7–8.
71. Rossetti, G., A. Magistrato, A. Pastore, F. Persichetti, and P. Carloni. 2008. Structural Properties of Polyglutamine Aggregates Investigated via Molecular Dynamics Simulations. *J. Phys. Chem. B* 112:16843–16850.
72. Côté, S., G. Wei, and N. Mousseau. 2012. All-Atom Stability and Oligomerization Simulations of Polyglutamine Nanotubes with and without the 17-Amino-Acid N-Terminal Fragment of the Huntingtin Protein. *J. Phys. Chem. B* 116:12168–12179.
73. Nakano, M., H. Watanabe, S. M. Rothstein, and S. Tanaka. 2010. Comparative Characterization of Short Monomeric Polyglutamine

Peptides by Replica Exchange Molecular Dynamics Simulation. *J. Phys. Chem. B* 114:7056–7061.
74. Esposito, L., A. Paladino, C. Pedone, and L. Vitagliano. 2008. Insights into Structure, Stability, and Toxicity of Monomeric and Aggregated Polyglutamine Models from Molecular Dynamics Simulations. *Biophys. J.* 94:4031–4040.
75. Poirier, M. A., H. Jiang, and C. A. Ross. 2005. A structure-based analysis of huntingtin mutant polyglutamine aggregation and toxicity: evidence for a compact beta-sheet structure. *Hum. Mol. Genet.* 14:765–774.
76. Peters-Libeu, C., J. Miller, E. Rutenber, Y. Newhouse, P. Krishnan, K. Cheung, D. Hatters, E. Brooks, K. Widjaja, T. Tran, S. Mitra, M. Arrasate, L. A. Mosquera, D. Taylor, K. H. Weisgraber, and S. Finkbeiner. 2012. Disease-Associated Polyglutamine Stretches in Monomeric Huntingtin Adopt a Compact Structure. *J. Mol. Biol.* 421:587–600.
77. Kajava, A. V., U. Baxa, and A. C. Steven. 2010. β-arcades: recurring motifs in naturally occurring and disease-related amyloid fibrils. *FASEB J.* 24:1311–1319.
78. Sharma, D., L. M. Shinchuk, H. Inouye, R. Wetzel, and D. A. Kirschner. 2005. Polyglutamine homopolymers having 8–45 residues form slablike beta-crystallite assemblies. *Proteins* 61:398–411.

List of Figures

To assess when a given dimer replica lost its structure, we inspected all the 180 trajectories visually and calculated the center of mass distance (COMD) between the two monomers and the root mean squared deviation (RMSD) of all the backbone atoms as a function of time.

The β-sheet dimers were practically unaffected by a 100 ns simulation (Fig. S1). Similar behavior was observed for all the β-hairpin-containing dimers, as shown by the unchanging COMDs (Fig. S2) and small RMSDs (Fig. S3).

We found that an RMSD-limit of 0.25 nm described the disintegration of the structure well for all but the α-helical structures (Fig. S3). The α-helical monomers were able to roll on one another, which increased the RMSD, but did not qualitatively change the structure of the dimer, hence an RMSD-limit of 1.0 nm was found to be more appropriate; this was supplemented by a COMD-limit of 2.0 nm to pinpoint the events in which the two helices separated (Fig. S4). In addition to the α-helix dimers, the separation of peptides was only observed once, in a CHARMM27 replica of the β-nanotube dimer (Fig. S5).

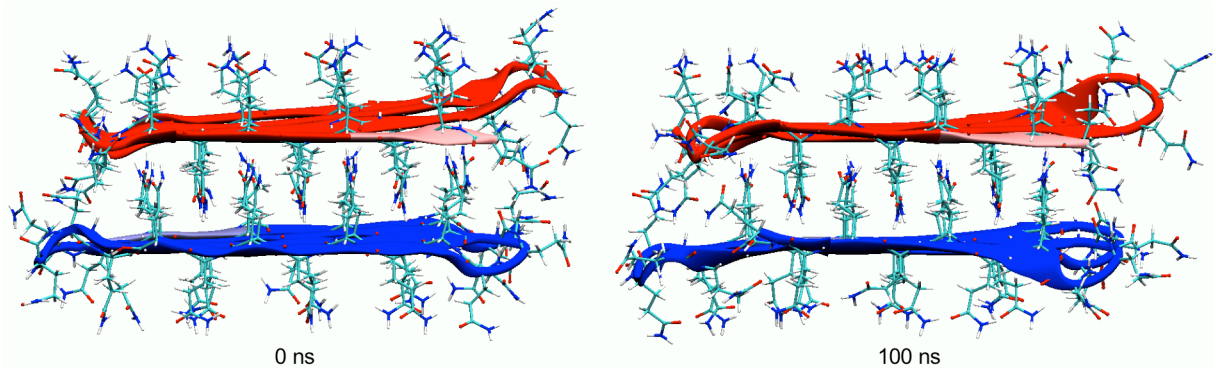

FIG. S1: In the β-sheet dimer the side chains of the monomers interdigitated. The resulting structure was thus stabilized by intra-peptide backbone–backbone hydrogen bonds in one direction and inter-peptide side chain–side chain interdigitation in the other. The same motif occurs in the β-sheetstack conformer. The structure was very stable, experiencing practically no changes in a 100 ns simulation.

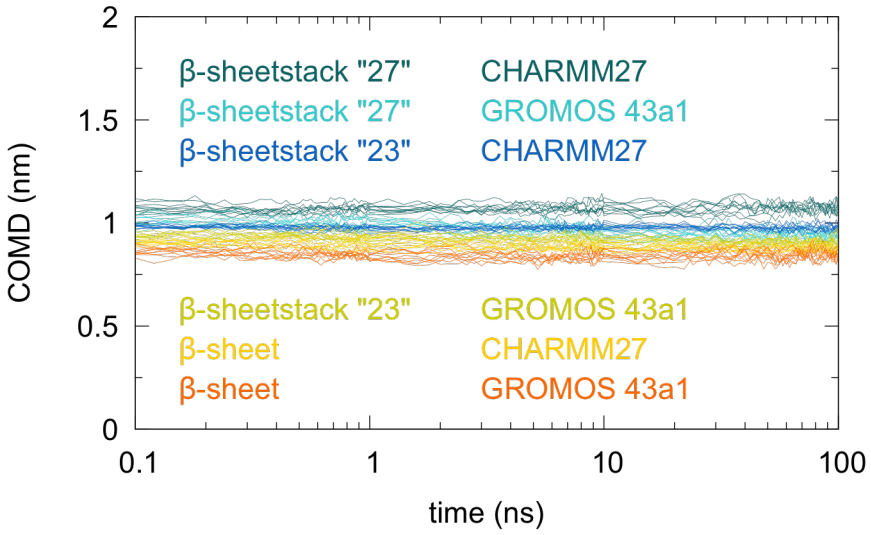

FIG. S2: The peptide–peptide center of mass distance (COMD) as a function of simulation time in the 60 simulations of β-hairpin-containing dimers. The numbers "23" and "27" refer to the two orientations of monomers for the β-sheetstack dimer, see Fig. 2.

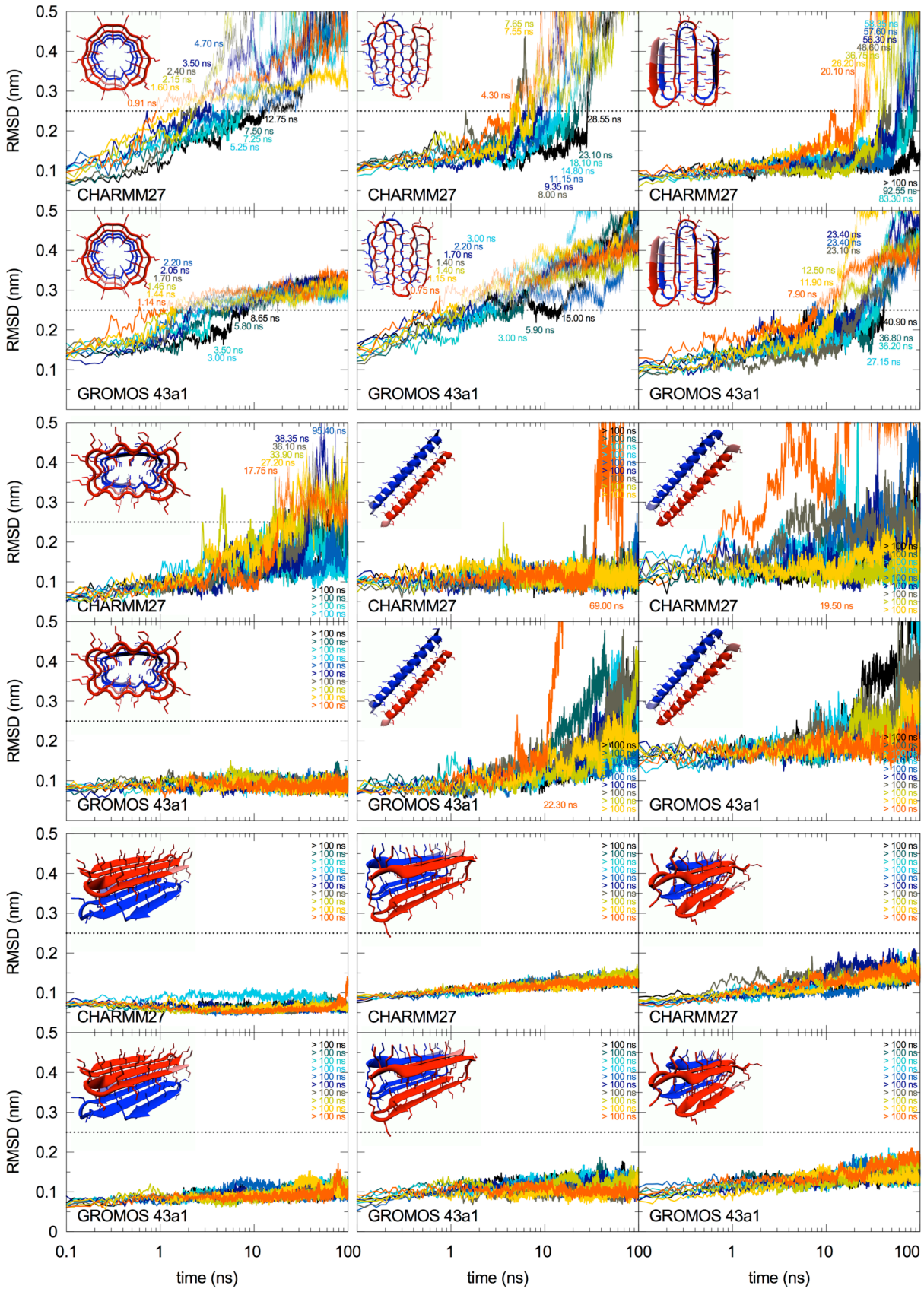

FIG. S3: The root mean squared deviation (RMSD) of backbone atoms for all the 180 simulations. The snapshots show the initial structures. The dotted line at 0.25 nm shows the limit beyond which the dimer was considered to have lost its initial structure. For α-helix dimers this limit was set to 1.0 nm. The colored numbers are the disintegration times of their respective replicas.

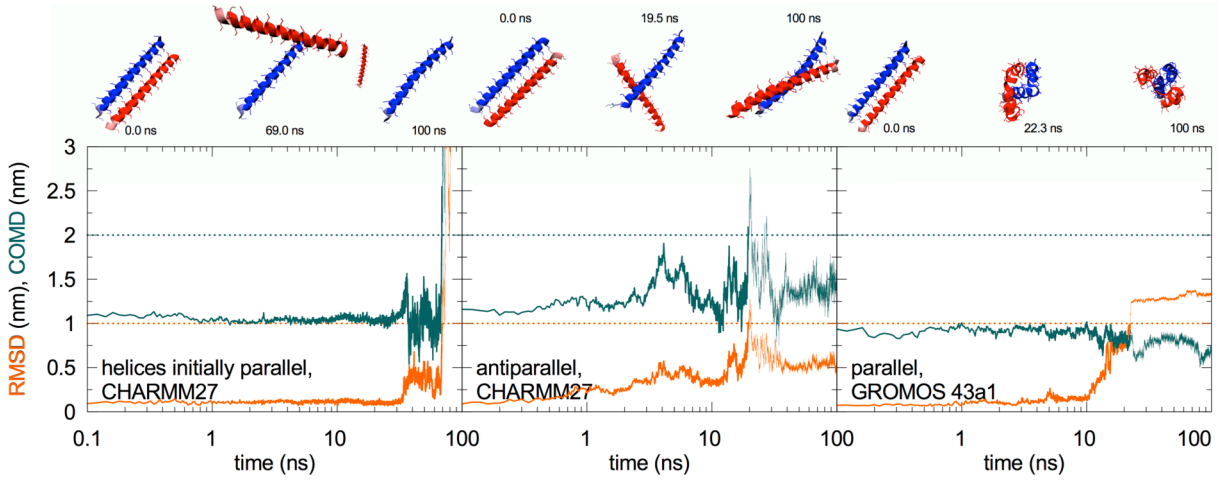

FIG. S4: The breaking events observed for α-helix dimers comprised two cases where the monomers separated while staying α-helical (left and middle panel) and one case where they collapsed while staying together (right).

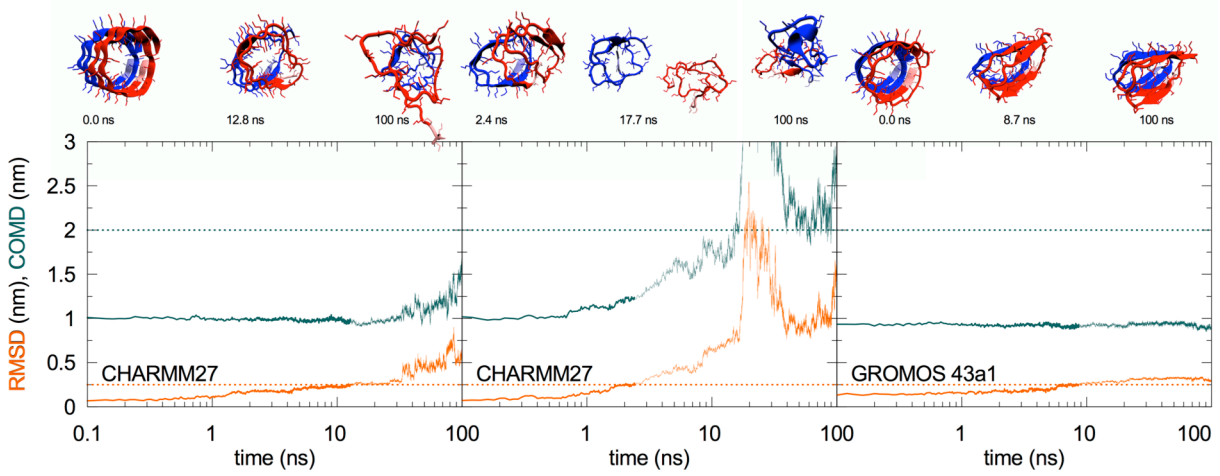

FIG. S5: Examples of breaking events observed for the β-nanotube dimers. With the CHARMM27 force field, the initial structure was always lost to a great extent, but the monomers stayed together (left panel) except for one replica, which after essentially unfolding at 2.4 ns also experienced separation of the peptides at 17.7 ns (middle). With GROMOS 43a1, the initial structure was typically lost by squeezing of the nanotube, leading to a configuration resembling the dry-core β-pseudohelix (right).